Data-Driven Motion-Force Control Scheme for Redundant Manipulators: A Kinematic Perspective

Jialiang Fan, Long Jin, *Senior Member, IEEE*, Zhengtai Xie, Shuai Li, *Senior Member, IEEE*, and Yu Zheng, *Senior Member, IEEE*

***Abstract*—Redundant manipulators play a critical role in industry and academia, which can be controlled from the kinematic or dynamic perspective. The motion-force control of redundant manipulators is a core problem in robot control, especially for the task requiring keeping contact with objectives, such as cutting, polishing, deburring, etc. However, when a manipulator's model structure is unknown, it is challenging to take motion-force control of redundant manipulators. This article proposes a data-driven-based motion-force control scheme, which solves the motion-force control problem from the kinematic perspective. The scheme can take effect and estimate the structure information, i.e., the model parameters involved in the forward kinematics when the structure of the manipulator is incomplete or unknown. A recurrent neural network is devised to find the solution to the scheme. Besides, the theoretical analysis is presented to prove the correctness of the scheme. Simulations and physical experiments running on seven degrees of freedom redundant manipulators illustrate the superb performance and practicability of the scheme intuitively. The key contribution of this article is that, for the first time, a motion-force control scheme aided with data-driven technology is proposed from a kinematic perspective for the redundant manipulators.**

***Index Terms*—Data driven, kinematic control, motion-force control, recurrent neural network (RNN), redundant manipulators.**

Manuscript received September 11, 2021; revised October 15, 2021 and October 29, 2021; accepted October 31, 2021. Date of publication November 8, 2021; date of current version May 6, 2022. This work was supported in part by the National Natural Science Foundation of China under Grant 62176109, in part by CIE-Tencent Robotics X Rhino-Bird Focused Research Program under Grant 2021-01, in part by the Natural Science Foundation of Chongqing, China, under Grant cstc2020jcyj-zdxmX0028, in part by the Chinese Academy of Sciences "Light of West China" Program, in part by the Natural Science Foundation of Gansu Province under Grant 21JR7RA531 and Grant 20JR10RA639, in part by the CAAI-Huawei MindSpore Open Fund, China, under Grant CAAIXSJLJJ-2020-012 A, in part by the Gansu Provincial Youth Doctoral Fund of Colleges and Universities under Grant 2021QB-003, in part by the Fundamental Research Funds for the Central Universities under Grant lzujbky-2021-65, in part by the Education Department of Gansu Province: Excellent Graduate student "Innovation Star" project under Grant 2021CXZX-120, and in part by the Supercomputing Center of Lanzhou University. Paper no. TII-21-3931. *(Jialiang Fan and Long Jin are co-first authors.) (Corresponding author: Long Jin.)*

Jialiang Fan is with the School of Information Science and Engineering, Lanzhou University, Lanzhou 730000, China, and also with the Academy of Plateau Science and Sustainability, Xining 810016, China (e-mail: fjl2401@163.com).

Long Jin is with the Chongqing Key Laboratory of Big Data and Intelligent Computing, Chongqing Institute of Green and Intelligent Technology, Chinese Academy of Sciences, Chongqing 400714, China, and also with the Department of Computer Science, Lanzhou University, Lanzhou 730000, China (e-mail: jinlongsysu@foxmail.com).

Zhengtai Xie and Shuai Li are with the School of Information Science and Engineering, Lanzhou University, Lanzhou 730000, China (e-mail: xzt1xzt@vip.qq.com; lishuai@lzu.edu.cn).

Yu Zheng is with Tencent, Robotics X, Shenzhen 518057, China (e-mail: petezheng@tencent.com).

Color versions of one or more figures in this article are available at https://doi.org/10.1109/TII.2021.3125449.

Digital Object Identifier 10.1109/TII.2021.3125449

I. Introduction

REDUNDANT manipulators are one of the most widely used robots in the industrial and academic fields. Compared to conventional industrial robots, redundant manipulators have more degrees of freedom (DOF) than the given task required. The extra DOFs can be utilized to fulfill the secondary tasks, such as obstacle avoidance, singularity avoidance, minimizing the system energy consumption [1], etc., but also increase the difficulty of finding the efficient control resolution.

Motion control and force control are two different aspects of manipulator control. Motion control assumes that the robot has no touch with the object in the workspace, which means that the robot will precisely move along the predefined trajectory. Hence, motion control's core problem is calculating the real-time control commands to drive the manipulator to move along the predefined trajectory. The manipulator can be controlled in the joint and Cartesian spaces from the angular, velocity, or acceleration perspectives [2], [3]. In recent years, there are plenty of meaningful works on the motion control of redundant manipulators. Zhang and Yan [4] investigate the motion planning problem of redundant manipulators from an optimization perspective. The control problem is finally transformed into a quadratic programming (QP) problem, which is solved by a varying parameter recurrent neural network [4].

By contrast, force control is different from the motion control of the manipulator. When using force control, there is a direct interaction between the object and the manipulator. Thus, the contact force will be adjusted by measuring the contact force between the manipulator and the environment. The applications of force control in the industry can be cutting [5], polishing [6], deburring [7], etc.

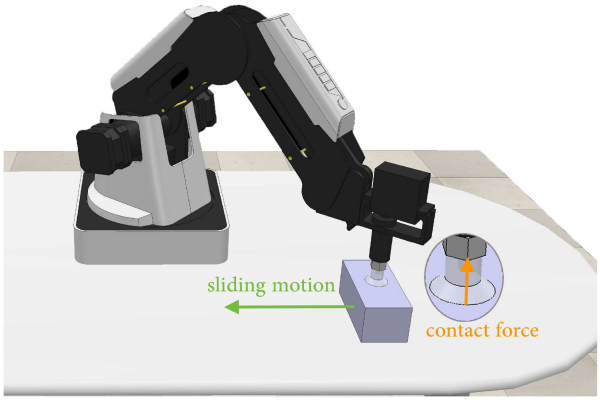

Fig. 1. Schematic of a simple motion-force control of the Dobot Magician manipulator.

Hybrid motion-force control is usually a more feasible approach in many practical applications compared to the single control scheme. For example, under the circumstance of pure motion control, once the robot encounters obstacles during its movements, the position tracking error will increase dramatically. At this point, the manipulator will attempt to track the desired trajectory, which may eventually cause a substantial internal force between the manipulator and the obstacle and cause damage to the manipulator or internal components. However, in the condition of motion-force control, one of the task's goals is to control the force between the manipulator and obstacles. When the manipulator encounters an obstacle, it intelligently adjusts the preset position trajectory to eliminate internal forces. There have been plenty of studies on motion-force control in the past few years. In [8], a novel adaptive control method based on the admittance model is presented for the cooperative control of multiple manipulators to transport an object along a predefined trajectory. The resolution is built on a dynamic perspective with robot kinematics consideration, which can be seen as the hybrid motion-force control.

Although the works mentioned above have made great success in motion-force control of manipulators, their research mainly focuses on the dynamic perspective. In recent years, dealing with motion-force control problems from a kinematic perspective based on the idea of admittance control has become increasingly prevalent [9]. Especially in the practical applications that are not necessary to control the contact force in all directions, like polishing and assembly. For example, Fig. 1 describes a motion-force control scenario that the force control works in a direction perpendicular to the object plane, where there is a constant pressure. While in the direction parallel to the object plane, the primary purpose is to ensure that the manipulator's trajectory obeys the predefined path. Xu *et al.* [9] present a motion-force control scheme from a kinematic perspective, which means that the force on the end-effector is generated by the end-effector displacement during the kinematic control. In the meantime, physical constraints and torque optimization are incorporated into the scheme, and the control problem is finally turned into a QP problem [9]. Considering the motion-force control of manipulators from a kinematic perspective is rarely studied and worthy of further study, this article aims at finding a kinematic resolution to address the motion-force control problem. Besides, in many realistic scenarios, the manipulators' parameters during the control are potentially inaccurate or unknown, making the control of the manipulator challenging. An effective method for dealing with this problem is utilizing the known information to estimate the required parameters online. Li *et al.* [10] present a model-free dual network for addressing the redundancy resolution of manipulators, and no prior knowledge of the manipulator is required.

Considering that most existing works on motion-force control of the manipulator require structure information, this article proposes a data-driven-based motion-force control (DDMFC) scheme for redundant manipulators from a kinematic perspective. In the meantime, physical constraints and end-effector orientation maintenance are taken into account with practical application requirements. Besides, a recurrent neural network (RNN) is devised to find the DDMFC scheme's solution, simultaneously solving learning problems and control problems.

The rest of this article is organized as follows. Section II introduces the redundant manipulator's fundamental kinematic conceptions and gives a brief introduction of the data-driven learning formula. In Section III, a generalized motion-force control problem is set up and formulated, and the RNN based method is presented. In Section IV, the DDMFC scheme is finally devised, with the combination of learning and control parts, and then, the corresponding theoretical analysis proves the feasibility of the proposed scheme. Simulation results, physical experiments, and comparisons of the DDMFC scheme are presented in Section V.

Finally, Section VI concludes this article. Before ending this section, the main contributions of this article are summarized as follows.

1) For the first time, the motion-force control problem of the redundant manipulator is investigated from a kinematic perspective with the manipulator's structure unknown, and the DDMFC scheme is formulated.
2) For protecting the manipulator and realistic application requirements, the physical constraints and end-effector orientation maintenance are considered in the scheme.
3) By applying the DDMFC scheme to seven-DOF manipulators, the scheme's correctness and effectiveness are proved, and the comparisons with other controllers also demonstrate the novelty of the proposed scheme.

II. Preliminaries

The coordinate transformation from joint space to Cartesian space of a manipulator is usually called the forward kinematics problem. The D-H parameters describe the manipulator's structure, which is exploited by researchers for generalizing the forward kinematics of the manipulator. The coordinate transformation of a redundant manipulator from the joint coordinate $\mathbf{q} \in \mathbb{R}^a$ to the Cartesian coordinate $\mathbf{p} \in \mathbb{R}^b (a > b)$ is described as

$$\Phi(\mathbf{q}) = \mathbf{p} \tag{1}$$

where $\Phi(\cdot)$ is a nonlinear mapping describing the forward kinematics, which is difficult to solve directly. Taking the time derivative to both sides of (1) results in the following:

$$J(\mathbf{q})\dot{\mathbf{q}} = \dot{\mathbf{p}} \tag{2}$$

where $J(\mathbf{q}) = \partial\Phi(\mathbf{q})/\partial\mathbf{q} \in \mathbb{R}^{b\times a}$ is the Jacobian matrix of $\Phi(\cdot)$; $\dot{\mathbf{q}}$ and $\dot{\mathbf{p}}$ are the joint and end-effector velocities of the manipulator, respectively. Hereto, the coordinate transformation problem is converted to an affine system. Besides, manipulators usually have physical limits during task execution in reality. To protect the motors of the manipulator, the limits of the joint position and velocity are considered simultaneously, which can be written as

$$\boldsymbol{\zeta}^{-}(t) \le \dot{\mathbf{q}}(t) \le \boldsymbol{\zeta}^{+}(t) \tag{3}$$

where $\boldsymbol{\zeta}^{-}(t) = \max\{\dot{\mathbf{q}}^{-}, \alpha(\mathbf{q}^{-} - \mathbf{q}(t))\}$ and $\boldsymbol{\zeta}^{+}(t) = \min\{\dot{\mathbf{q}}^{+}, \alpha(\mathbf{q}^{+} - \mathbf{q}(t))\}$; $\dot{\mathbf{q}}^{-}$ and $\dot{\mathbf{q}}^{+}$ represent the upper and lower bounds of the joint velocity, respectively; $\mathbf{q}^{-}$ and $\mathbf{q}^{+}$ represent the upper and lower bounds of the joint position, respectively; $\alpha > 0 \in \mathbb{R}$ is utilized to scale the feasible region of $\dot{\mathbf{q}}$.

It is worth pointing out that the existing work is usually based on the assumption that the structure information of the manipulator is known, such as the D-H parameters in (1) and the Jacobian matrix in (2). In this regard, when the parameters of a manipulator are unknown, it is impossible to control it in accordance with the above formula (2). Hence, this article endeavors to investigate the motion-force control of a manipulator with unknown model structure information, and the estimation of the Jacobian matrix based on data-driven technology is presented as

$$\tilde{J}\dot{\mathbf{q}} = \bar{\dot{\mathbf{p}}} \tag{4}$$

where $\tilde{J}$ represents the estimated Jacobian matrix; $\bar{\dot{\mathbf{p}}}$ represents the calculated results of actual end-effector velocity based on the estimated Jacobian matrix. When $\tilde{J}$ approaches J or even equals J, $\bar{\dot{\mathbf{p}}}$ approximately equals $\dot{\mathbf{p}}$. For obtaining an accurate estimate of the Jacobian matrix, an error function $\psi = ||\bar{\dot{\mathbf{p}}} - \dot{\mathbf{p}}||_2^2/2$ is defined and minimized by the gradient descent method [11] where $||\cdot||_2$ represents the 2-norm of a vector. Taking the partial derivative of the error function with respect to $\tilde{J}$ results in

$$\varpi\dot{\tilde{J}} = -\frac{\partial\psi}{\partial\tilde{J}} = -(\bar{\dot{\mathbf{p}}} - \dot{\mathbf{p}})\dot{\mathbf{q}}^{\mathrm{T}} = (\dot{\mathbf{p}} - \tilde{J}\dot{\mathbf{q}})\dot{\mathbf{q}}^{\mathrm{T}} \tag{5}$$

where ϖ is a teeny-tiny value, representing the step-size of each iteration, and $\dot{\tilde{J}}$ represents the derivative of $\tilde{J}$. It can be seen from (5) that the essence of data-driven technology lies in calculating $\dot{\tilde{J}}$ by measuring the real-time actual joint velocity $\dot{\mathbf{q}}$ and actual end-effector velocity $\dot{\mathbf{p}}$. In addition, since (5) does not involve the real Jacobian matrix J, it can be calculated without the real structure information.

III. Problem Formulation

In this section, the motion-force control problem of redundant manipulators is formulated from the kinematic perspective. The objective function is defined to minimize the norm of the joint velocity for saving the energy consumption of the redundant manipulator control. Keeping the position and orientation of the end-effector and satisfying other physical constraints are considered as secondary tasks. Furthermore, an RNN based resolution is constructed.

A. Motion-Force Control Problem Formulation

Fig. 1 simply depicts a motion-control task on the Dobot Magician manipulator. To achieve the task, one needs to control the normal contact force, which is perpendicular to the object plane. Simultaneously, the manipulator's end-effector interacts directly with the object, and the contact force is generated in the direction perpendicular to the surface due to the object's deformation on the surface. Let $\mathbf{s}_{\mathrm{e}} = \mathbf{p} - \mathbf{p}_{\mathrm{d}}$ be the displacement of object's surface in the end-effector coordinate system, where $\mathbf{p}_{\mathrm{d}}$ is the desired end-effector position. The relation between the contact force and the displacement can be written as

$$\mathbf{f}_{\mathrm{e}} = \eta\Delta\mathbf{s}_{\mathrm{e}} \tag{6}$$

where $\eta > 0$ is the stiffness coefficient of the object surface; $\mathbf{f}_{\mathrm{e}}$ represents the contact force in the end-effector coordinate system; $\Delta = \mathrm{diag}(0, 0, 1)$ decomposes the contact force along X, Y, and Z axes. Without loss of generality, this article considers the contact force along the Z-axis. Similarly, the position tracking error in the end-effector coordinate system is written as

$$\boldsymbol{e}_{\mathrm{e}} = \bar{\Delta}\mathbf{s}_{\mathrm{e}} \tag{7}$$

where $\bar{\Delta} = I - \Delta = \mathrm{diag}(1, 1, 0)$, in which 1 and 0 represent that the manipulator can and cannot move along the corresponding direction, respectively. When the contact surface is predefined, the contact force $\mathbf{f}_{\mathrm{e}}$, the position tracking error $\boldsymbol{e}_{\mathrm{e}}$, and the displacement $\mathbf{s}_{\mathrm{e}}$ can be transformed into the base coordinate system by the rotation matrix $R \in SO(3)$ as $\mathbf{f}_{\mathrm{b}} = R^{\mathrm{T}}\mathbf{f}_{\mathrm{e}}$, $\boldsymbol{e}_{\mathrm{b}} = R^{\mathrm{T}}\boldsymbol{e}_{\mathrm{e}}$, and $\mathbf{s}_{\mathrm{b}} = R^{\mathrm{T}}\mathbf{s}_{\mathrm{e}}$, where $\mathbf{f}_{\mathrm{b}}$, $\boldsymbol{e}_{\mathrm{b}}$, and $\mathbf{s}_{\mathrm{b}}$ represent the descriptions of $\mathbf{f}_{\mathrm{e}}$, $\boldsymbol{e}_{\mathrm{e}}$, and $\mathbf{s}_{\mathrm{e}}$ with respect to the base coordinate system, respectively. Then, $\mathbf{f}_{\mathrm{b}}$ and $\boldsymbol{e}_{\mathrm{b}}$ can be reformulated as [9]

$$\begin{cases} \mathbf{f}_{\mathrm{b}} = \eta R^{\mathrm{T}}\Delta R\mathbf{s}_{\mathrm{b}} \\ \boldsymbol{e}_{\mathrm{b}} = R^{\mathrm{T}}\bar{\Delta}R\mathbf{s}_{\mathrm{b}} \end{cases}. \tag{8}$$

Remark 1: Equation (8) describes the relationship of end-effector displacement $\mathbf{s}_{\mathrm{b}}$, contact force $\mathbf{f}_{\mathrm{b}}$, and tracking error $\boldsymbol{e}_{\mathrm{b}}$ in the base coordinate system. Besides, the contact force on the end-effector is determined by both the stiffness coefficient η and the displacement $\mathbf{s}_{\mathrm{e}}$, and finally decoupled by the diagonal matrix Δ along different axes.

The end-effector error $\boldsymbol{e}_{\mathrm{e}}$ can also be decoupled by $\bar{\Delta}$, that is, $\boldsymbol{e}_{\mathrm{e}}$ works on X- and Y-axes. When the contact force $\mathbf{f}_{\mathrm{d}}$ between the end-effector and the object is specified in practical applications, the control goal is to maintain $\mathbf{f}_{\mathrm{d}}$ on the object, and the position tracking error $\boldsymbol{e}_{\mathrm{e}}$ should converge to zero, that is, $\mathbf{f}_{\mathrm{e}} \to \mathbf{f}_{\mathrm{d}}$ and $\boldsymbol{e}_{\mathrm{e}} \to 0$. For the convenience of writing, (8) can be rewritten as

$$A(\mathbf{p} - \mathbf{p}_{\mathrm{d}}) = \boldsymbol{r} \tag{9}$$

in which $A = [\eta R^{\mathrm{T}}\Delta R; R^{\mathrm{T}}\bar{\Delta}R] \in \mathbb{R}^{6\times 3}$, $\boldsymbol{r} = [\mathbf{f}_{\mathrm{b}}^{\mathrm{T}}, \boldsymbol{e}_{\mathrm{b}}^{\mathrm{T}}]^{\mathrm{T}}$, $\boldsymbol{r}_{\mathrm{d}} = [\mathbf{f}_{\mathrm{d}}; 0]$. It can be found from (9) that the control objective of manipulators is to let $\boldsymbol{r} \to \boldsymbol{r}_{\mathrm{d}}$ by adjusting the joint position $\mathbf{q}$. For saving the energy and keeping the manipulator stable during

task execution, $\dot{\mathbf{q}}^{\mathrm{T}}\dot{\mathbf{q}}/2$ is taken as the objective function, which means that, the less value of the objective function is, the less energy of the task consumes. Meanwhile, in many applications, the end-effector's orientation should keep constant when the manipulator interacts with the object. For example, when the manipulator executes a laser cutting task, the end-effector's orientation should be maintained with high accuracy. To this end, the rotation matrix R should be invariable during the task, which is presented as

$$R(t) = R(0) \tag{10}$$

where $R = [\mathbf{a}, \mathbf{b}, \mathbf{c}]$, and $\mathbf{a} = [a_1, a_2, a_3]^{\mathrm{T}}, \mathbf{b} = [b_1, b_2, b_3]^{\mathrm{T}}, \mathbf{c} = [c_1, c_2, c_3]^{\mathrm{T}}$ represent the normal vector, orientation vector, and approach vector, respectively. $R(0) \in SO(3)$ and $R(t) \in SO(3)$ represent the rotation matrix R at time 0 and time t, respectively. Since the rotation matrix R is an orthogonal matrix, once any two elements of each row or column are fixed, the row or column vector will be determined as well. In this article, the orientation vector is devised as follows:

$$\mathbf{w} = [b_2, b_3, c_2, c_3]^{\mathrm{T}}. \tag{11}$$

Considering that this article investigates the manipulator control problem on velocity level, taking the derivative of $\mathbf{w}$ results in $\dot{\mathbf{w}}(0) = \dot{\mathbf{w}}(t) = H\dot{\mathbf{q}} = 0$, where $H = \partial \mathbf{w}/\partial \mathbf{q} \in \mathbb{R}^{4\times n}$ is the Jacobian matrix of $\mathbf{w}$[12]. In this case, the orientation of end-effector keeps the initial state during the procession.

The physical constraints given by (3) are also taken into consideration for protecting the manipulator. Combining the abovementioned, we conclude the following scheme:

$$\min \quad \dot{\mathbf{q}}^{\mathrm{T}}\dot{\mathbf{q}}/2 \tag{12a}$$

$$\text{s.t.} \quad \boldsymbol{r}_{\mathrm{d}} = A(\mathbf{p} - \mathbf{p}_{\mathrm{d}}) \tag{12b}$$

$$H\dot{\mathbf{q}} = 0 \tag{12c}$$

$$\dot{\mathbf{q}}(t) \in \Omega \tag{12d}$$

where $\Omega = \{\dot{\mathbf{q}} \in \mathbb{R}^n | \boldsymbol{\zeta}^-(t) \le \dot{\mathbf{q}} \le \boldsymbol{\zeta}^+(t)\}$. To get the solution of the scheme, the equality constraints (12b) need to be reconstructed at the velocity level, because the mapping from joint space to Cartesian space is usually nonlinear and difficult to solve directly. To rewrite (12b), first, define a vector $\boldsymbol{e} = \boldsymbol{r} - \boldsymbol{r}_{\mathrm{d}} = [\mathbf{f}_{\mathrm{b}} - \mathbf{f}_{\mathrm{d}}; \boldsymbol{e}_{\mathrm{b}}]$, which unifies the force error and position error; then, from (9), $\boldsymbol{e}$ can be written as $\boldsymbol{e} = A(\mathbf{p} - \mathbf{p}_{\mathrm{d}}) - \boldsymbol{r}_{\mathrm{d}}$. Taking the derivation to both sides of the equation leads to

$$\dot{\boldsymbol{e}} = A(J\dot{\mathbf{q}} - \dot{\mathbf{p}}_{\mathrm{d}}) - \dot{\boldsymbol{r}}_{\mathrm{d}}. \tag{13}$$

To make sure that the error can converge to zero, a neural dynamics design method $\dot{\boldsymbol{e}} = -k\boldsymbol{e}$ is designed [13]; $k > 0$ is a constant, and the equality constraints (12b) are transformed to the velocity level based on (13). Finally, we derive

$$AJ\dot{\mathbf{q}} = \dot{\boldsymbol{r}}_{\mathrm{d}} + A(\dot{\mathbf{p}}_{\mathrm{d}} - k(\mathbf{p} - \mathbf{p}_{\mathrm{d}})) + k\boldsymbol{r}_{\mathrm{d}}. \tag{14}$$

For presentation convenience, let $W = \dot{\boldsymbol{r}}_{\mathrm{d}} + A(\dot{\mathbf{p}}_{\mathrm{d}} - k(\mathbf{p} - \mathbf{p}_{\mathrm{d}})) + k\boldsymbol{r}_{\mathrm{d}}$, and then, (14) is rewritten as

$$AJ\dot{\mathbf{q}} = W. \tag{15}$$

Hereto, the scheme formulation for the motion-force control problem of the redundant manipulator is finished.

B. RNN-Based Resolution

From (12) and the above discussions, the motion-force control scheme at the velocity level is formulated as

$$\min \quad \dot{\mathbf{q}}^{\mathrm{T}}\dot{\mathbf{q}}/2 \tag{16a}$$

$$\text{s.t.} \quad AJ\dot{\mathbf{q}} = W \tag{16b}$$

$$H\dot{\mathbf{q}} = 0 \tag{16c}$$

$$\dot{\mathbf{q}} \in \Omega. \tag{16d}$$

To solve the optimization problem (16), an RNN is designed as follows. First, we establish a Lagrange function as

$$L = \dot{\mathbf{q}}^{\mathrm{T}}\dot{\mathbf{q}}/2 + \boldsymbol{\lambda}_1^{\mathrm{T}}(AJ\dot{\mathbf{q}} - W) + \boldsymbol{\lambda}_2^{\mathrm{T}}H\dot{\mathbf{q}} \tag{17}$$

where $\boldsymbol{\lambda}_1 \in \mathbb{R}^{2b}$ and $\boldsymbol{\lambda}_2 \in \mathbb{R}^4$ are the Lagrange multipliers corresponding to equality constraints (16b) and (16c). Then, taking the partial derivatives to $\dot{\mathbf{q}}$, $\boldsymbol{\lambda}_1$, and $\boldsymbol{\lambda}_2$ of (17), respectively, we obtain

$$\frac{\partial L}{\partial \dot{\mathbf{q}}} = \dot{\mathbf{q}} + J^{\mathrm{T}}A^{\mathrm{T}}\boldsymbol{\lambda}_1 + H^{\mathrm{T}}\boldsymbol{\lambda}_2 = 0 \tag{18a}$$

$$\frac{\partial L}{\partial \boldsymbol{\lambda}_1} = AJ\dot{\mathbf{q}} - W = 0 \tag{18b}$$

$$\frac{\partial L}{\partial \boldsymbol{\lambda}_2} = H\dot{\mathbf{q}} = 0. \tag{18c}$$

It is worth mentioning that (18) is nonlinear, and difficult to solve directly. Therefore, from (18) we derive an RNN in the form of ordinary differential equation as

$$\delta\ddot{\mathbf{q}} = -\dot{\mathbf{q}} + \mathrm{P}_{\Omega}(-J^{\mathrm{T}}A^{\mathrm{T}}\boldsymbol{\lambda}_1 - H^{\mathrm{T}}\boldsymbol{\lambda}_2) \tag{19a}$$

$$\delta\dot{\boldsymbol{\lambda}}_1 = AJ\dot{\mathbf{q}} - W \tag{19b}$$

$$\delta\dot{\boldsymbol{\lambda}}_2 = H\dot{\mathbf{q}} \tag{19c}$$

where $0 < \delta < 1$ is used to regulate the convergence rate of the RNN, and the inequality constraints (12d) are reconstructed as a projection function $\mathrm{P}_{\Omega}(\mathbf{x}) = \arg\min_{\mathbf{y}\in\Omega}||\mathbf{x} - \mathbf{y}||_2$, which guarantees the boundness of joint velocity. From the above discussions, an RNN for solving the motion-force control problem is devised, maintaining the end-effector's orientation subject to the physical constraints, which has practical significance in real scenarios.

IV. Schemes, RNN, and Theoretical Analysis

In this section, a DDMFC scheme is presented, which combines a learning part and a control part. Besides, the RNN is reconstructed for the DDMFC scheme. Finally, the theoretical analysis is presented to prove the correctness of the scheme.

A. DDMFC Scheme

Revisiting that when the manipulator's structure information is unknown, the control of the manipulator will become tough. Therefore, this article proposes the DDMFC scheme to address

this problem. To establish the scheme, first, we replace the actual Jacobian matrix J in (16d) with the estimated Jacobian matrix $\tilde{J}$ in (5). Then, add (5) as a equality constraint of the scheme, and the scheme is deduced as follows:

$$\min \quad \dot{\mathbf{q}}^{\mathrm{T}}\dot{\mathbf{q}}/2 \tag{20a}$$

$$\text{s.t.} \quad A\tilde{J}\dot{\mathbf{q}} = W \tag{20b}$$

$$H\dot{\mathbf{q}} = 0 \tag{20c}$$

$$\varpi\dot{\tilde{J}} = (\dot{\mathbf{p}} - \tilde{J}\dot{\mathbf{q}})\dot{\mathbf{q}}^{\mathrm{T}} \tag{20d}$$

$$\dot{\mathbf{q}} \in \Omega. \tag{20e}$$

It is worth mentioning that the structure of the redundant manipulator is estimated by learning law (20d), which calculates the value of $\tilde{J}$ by measuring real-time end-effector velocities and joint velocities. Hereto, the DDMFC scheme (20) is successfully constructed.

B. Reconstruction of RNN

To find a solution to the scheme, both of the learning part and the control part need to be considered. Combining the data-driven solution (5) and motion-force control solution (19) results in

$$\delta\ddot{\mathbf{q}} = -\dot{\mathbf{q}} + \mathrm{P}_{\Omega}(-J^{\mathrm{T}}A^{\mathrm{T}}\boldsymbol{\lambda}_1 - H^{\mathrm{T}}\boldsymbol{\lambda}_2) \tag{21a}$$

$$\delta\dot{\boldsymbol{\lambda}}_1 = A\tilde{J}\dot{\mathbf{q}} - W \tag{21b}$$

$$\delta\dot{\boldsymbol{\lambda}}_2 = H\dot{\mathbf{q}} \tag{21c}$$

$$\varpi\dot{\tilde{J}} = (\dot{\mathbf{p}} - \tilde{J}\dot{\mathbf{q}})\dot{\mathbf{q}}^{\mathrm{T}}. \tag{21d}$$

Noting that there exists a special case that, if $\dot{\mathbf{q}}$, $\dot{\mathbf{p}}$ and $\tilde{J}(0)$ equal to zero at the initial state, the value of other variables in (21) can be conducted immediately: $\tilde{J} = 0, \dot{\boldsymbol{\lambda}}_1 = 0, \dot{\boldsymbol{\lambda}}_2 = 0$, and $\ddot{\mathbf{q}} = 0$. The system will be in a dilemma that the input data and the output data are zero all the time. To address the dilemma, an independent identically distributed noise $\mathbf{c}$ whose standard deviation is σ and $0 \le ||\mathbf{c}|| \le \mathbf{c}_0$ with $\mathbf{c}_0 > 0$ is added to the joint velocity intentionally as the activation signal, with $||\cdot||$ being the 2-norm of a vector. Furthermore, $\dot{\mathbf{q}}$ polluted by $\mathbf{c}$ is replaced with $\bar{\dot{\mathbf{q}}}$, and then the RNN is rewritten as

$$\delta\dot{\bar{\mathbf{q}}} = -\bar{\dot{\mathbf{q}}} + \mathrm{P}_{\Omega}(-J^{\mathrm{T}}A^{\mathrm{T}}\boldsymbol{\lambda}_1 - H^{\mathrm{T}}\boldsymbol{\lambda}_2) \tag{22a}$$

$$\delta\dot{\boldsymbol{\lambda}}_1 = A\tilde{J}\bar{\dot{\mathbf{q}}} - W \tag{22b}$$

$$\delta\dot{\boldsymbol{\lambda}}_2 = H\bar{\dot{\mathbf{q}}} \tag{22c}$$

$$\varpi\dot{\tilde{J}} = (J\dot{\mathbf{q}} - \tilde{J}\dot{\mathbf{q}})\dot{\mathbf{q}}^{\mathrm{T}} \tag{22d}$$

$$\dot{\mathbf{q}} = \bar{\dot{\mathbf{q}}} + \mathbf{c} \quad \text{with} \quad ||\mathbf{c}|| \le \mathbf{c}_0. \tag{22e}$$

C. Theoretical Analysis

In this part, to prove the feasibility of the DDMFC scheme (20), the learning and control abilities of the RNN are analyzed, respectively.

Theorem 1: When employing RNN (22) to solve the DDMFC scheme (20), the corresponding estimation error of Jacobian matrix approaches zero globally, and neural control law (18) solves the motion-force control problem of redundant manipulators with global convergence to a steady state.

Proof: For the learning and control abilities, we divide two parts so as to explain separately.

Part one: the learning ability of the RNN (22).

The Jacobian error matrix can be represented as $\hat{J} = \tilde{J} - J$. We can use Frobenius norm $V = ||\hat{J}||_F^2/2 = \mathrm{tr}(\hat{J}\hat{J}^{\mathrm{T}})/2$ with $\mathrm{tr}(\cdot)$ being the trace of a matrix to measure the estimation error of Jacobian matrix. Taking derivate to both sides of V can obtain

$$\begin{aligned}
\dot{V} &= \mathrm{tr}(\dot{\hat{J}}\hat{J}^{\mathrm{T}}) \\
&= \mathrm{tr}\left(1/\varpi\hat{J}^{\mathrm{T}}(\dot{\mathbf{p}} - \tilde{J}\dot{\mathbf{q}})\dot{\mathbf{q}}^{\mathrm{T}}\right) \\
&= -\mathrm{tr}\left(1/\varpi\hat{J}^{\mathrm{T}}\hat{J}(\bar{\dot{\mathbf{q}}} + \mathbf{c})(\bar{\dot{\mathbf{q}}} + \mathbf{c})^{\mathrm{T}}\right) \\
&= -\mathrm{tr}\left((1/\varpi\hat{J}(\bar{\dot{\mathbf{q}}} + \mathbf{c}))^{\mathrm{T}}\hat{J}(\bar{\dot{\mathbf{q}}} + \mathbf{c})\right) \\
&= -1/\varpi\|\hat{J}(\bar{\dot{\mathbf{q}}} + \mathbf{c})\|_F^2 \\
&\le 0.
\end{aligned} \tag{23}$$

Since $V > 0$ and $\dot{V} \le 0$, we let $\dot{V} = 0$ according to LaSalle's invariant principle [16] as

$$\lim_{t\to\infty} \hat{J}(\bar{\dot{\mathbf{q}}} + \mathbf{c}) = 0. \tag{24}$$

Multiplying $(\bar{\dot{\mathbf{q}}} + \mathbf{c})\hat{J}^{\mathrm{T}}$ on both sides of (24,) we can compute the expected value as

$$\begin{aligned}
&E\left((\bar{\dot{\mathbf{q}}} + \mathbf{c})^{\mathrm{T}}\hat{J}^{\mathrm{T}}\hat{J}(\bar{\dot{\mathbf{q}}} + \mathbf{c})\right) \\
&= E\left(\mathrm{tr}\left(\hat{J}^{\mathrm{T}}\hat{J}(\bar{\dot{\mathbf{q}}} + \mathbf{c})(\bar{\dot{\mathbf{q}}} + \mathbf{c})^{\mathrm{T}}\right)\right) \\
&= \mathrm{tr}\left(E\left(\hat{J}^{\mathrm{T}}\hat{J}\bar{\dot{\mathbf{q}}}\bar{\dot{\mathbf{q}}}^{\mathrm{T}}\right)\right) + \mathrm{tr}\left(E\left(\hat{J}^{\mathrm{T}}\hat{J}\right)E\left(\mathbf{c}\mathbf{c}^{\mathrm{T}}\right)\right) \\
&\quad + \mathrm{tr}\left(E\left(\hat{J}^{\mathrm{T}}\hat{J}\bar{\dot{\mathbf{q}}}\right)E^{\mathrm{T}}(\mathbf{c})\right) + \mathrm{tr}\left(E\left(\bar{\dot{\mathbf{q}}}^{\mathrm{T}}\hat{J}^{\mathrm{T}}\hat{J}\right)E(\mathbf{c})\right) \\
&= \mathrm{tr}\left(E\left(\bar{\dot{\mathbf{q}}}^{\mathrm{T}}\hat{J}^{\mathrm{T}}\hat{J}\bar{\dot{\mathbf{q}}}\right)\right) + \sigma^2\,\mathrm{tr}\left(E\left(\hat{J}^{\mathrm{T}}\hat{J}\right)\right) \\
&= 0, \quad \text{as } t \to \infty
\end{aligned} \tag{25}$$

where $E(\cdot)$ stands for the mathematical expectation. Recall that $\mathbf{c}$ is a identically distributed independent noise for which $E(\mathbf{c}) = E^{\mathrm{T}}(\mathbf{c}) = 0$, and $\mathrm{tr}(AB) = \mathrm{tr}(BA)$ for any matrices A and B, where $\mathrm{tr}(\cdot)$ stands for the trace of a matrix. Thus, we can derive

$$\mathrm{tr}(E(\hat{J}^{\mathrm{T}}\hat{J})E(\mathbf{c}\mathbf{c}^{\mathrm{T}})) = \delta^2\,\mathrm{tr}(E(\hat{J}^{\mathrm{T}}\hat{J})) \tag{26a}$$

$$\mathrm{tr}(E(\hat{J}^{\mathrm{T}}\hat{J}\bar{\dot{\mathbf{q}}})E^{\mathrm{T}}(\mathbf{c}))) = 0 \tag{26b}$$

$$\mathrm{tr}\,E(\bar{\dot{\mathbf{q}}}^{\mathrm{T}}\hat{J}^{\mathrm{T}}\hat{J})E(\mathbf{c})) = 0. \tag{26c}$$

Equation (26) is used in the derivation of (25). Considering that $\mathrm{tr}(E(\bar{\dot{\mathbf{q}}}^{\mathrm{T}}\hat{J}^{\mathrm{T}}\hat{J}\bar{\dot{\mathbf{q}}})) \ge 0$ and $\sigma^2\,\mathrm{tr}(E(\hat{J}^{\mathrm{T}}\hat{J})) \ge 0$, we can deduce

$$\mathrm{tr}(E(\hat{J}^{\mathrm{T}}\hat{J})) = E(\mathrm{tr}(\hat{J}^{\mathrm{T}}\hat{J})) = E(||\hat{J}||_F^2) = 0 \quad \text{as } t \to \infty.$$

Therefore, we have

$$\tilde{J} - J \to 0, \quad \text{as } t \to \infty. \tag{27}$$

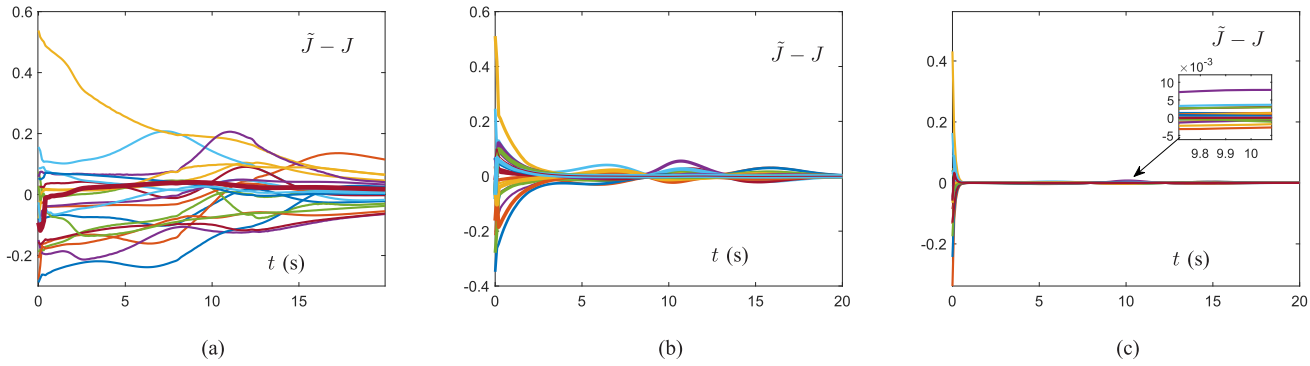

Fig. 2. Time history of Jacobian matrix estimation errors when employing different values of the step-size ϖ in the RNN (22). (a) With $\varpi = 10^{-4}$. (b) With $\varpi = 10^{-5}$. (c) With $\varpi = 10^{-6}$.

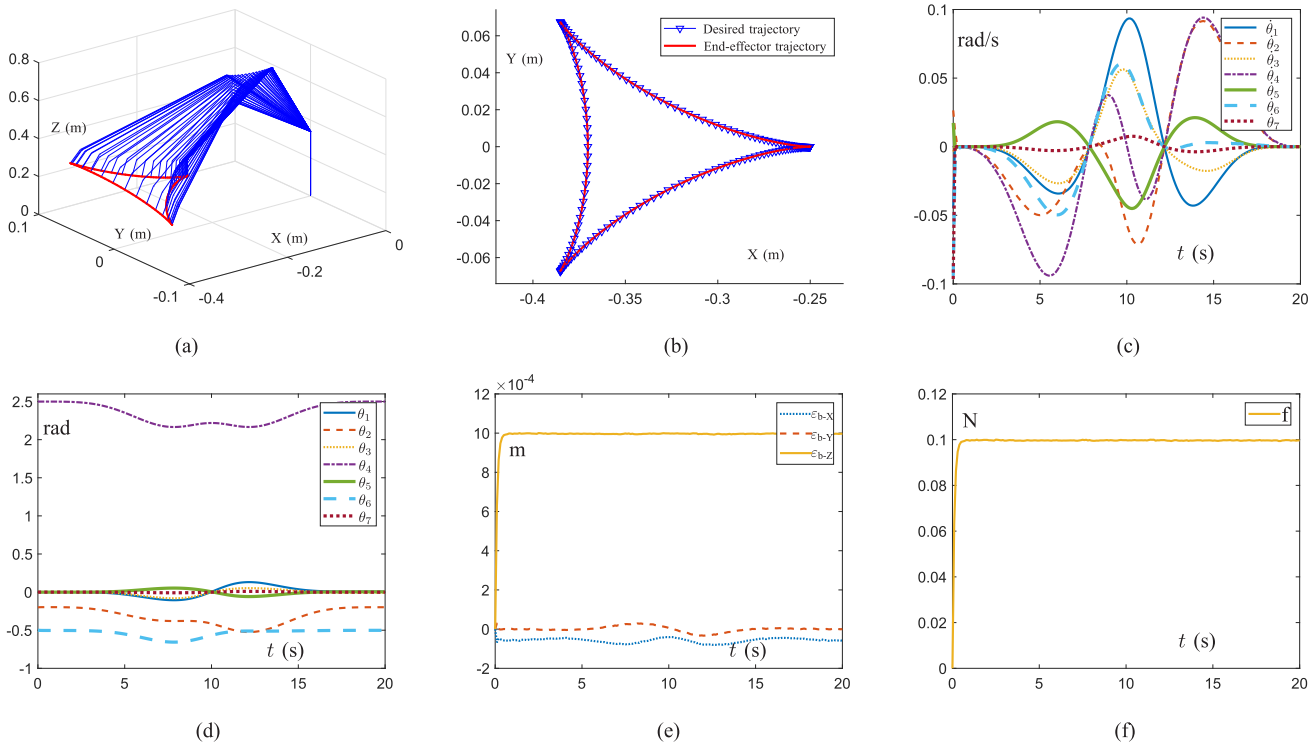

Fig. 3. Computer simulations on employing the DDMFC scheme (20) aided with RNN (22) to control the KUKA iiwa manipulator for tracking a tricuspid valve path. (a) Motion trajectory of the manipulator. (b) Real trajectory and desired trajectory of the endeffector. (c) Time history of the joint velocities of the manipulator with upper bound $\dot{\mathbf{q}}^{+} = 0.1$ rad/s and lower bound $\dot{\mathbf{q}}^{-} = -0.1$ rad/s. (d) Time history of joint angles. (e) Time history of position errors. (f) Time history of contact force on the end-effector along the *Z*-axis.

Hereto, the proof of RNN's learning ability is finished.

Part two: The control ability of the RNN (22): To prove the control ability of the RNN, first, by substituting $\hat{J} = \tilde{J} - J$ into (22), the neural dynamics of $\ddot{\mathbf{q}}$, $\dot{\boldsymbol{\lambda}}_1$, and $\dot{\boldsymbol{\lambda}}_2$ can be rewritten as

$$\delta\ddot{\mathbf{q}} = -\dot{\mathbf{q}} + \mathrm{P}_{\Omega}(-(J+\hat{J})^{\mathrm{T}}A^{\mathrm{T}}\boldsymbol{\lambda}_1 - H^{\mathrm{T}}\boldsymbol{\lambda}_1) \tag{28a}$$

$$\delta\dot{\boldsymbol{\lambda}}_1 = A(J+\hat{J})\dot{\mathbf{q}} - W \tag{28b}$$

$$\delta\dot{\boldsymbol{\lambda}}_2 = H\dot{\mathbf{q}}. \tag{28c}$$

Considering that the convergence of $\hat{J}$ has been proved in previous part, and according to LaSalle's invariant principle, the above formula can be rewritten as follows under the condition $\hat{J} = 0$:

$$\delta\ddot{\mathbf{q}} = -\dot{\mathbf{q}} + \mathrm{P}_{\Omega}(-J^{\mathrm{T}}A^{\mathrm{T}}\boldsymbol{\lambda}_1 - H^{\mathrm{T}}\boldsymbol{\lambda}_2) \tag{29a}$$

$$\delta\dot{\boldsymbol{\lambda}}_1 = AJ\dot{\mathbf{q}} - W \tag{29b}$$

$$\delta\dot{\boldsymbol{\lambda}}_2 = H\dot{\mathbf{q}}. \tag{29c}$$

For the convenience of analysing, by defining a new variable $\mathrm{u} = [\dot{\mathbf{q}}^{\mathrm{T}}, \boldsymbol{\lambda}_1^{\mathrm{T}}, \boldsymbol{\lambda}_2^{\mathrm{T}}]^{\mathrm{T}}$, thus, $\ddot{\mathbf{q}}$, $\dot{\boldsymbol{\lambda}}_1$, and $\dot{\boldsymbol{\lambda}}_2$ are unified to the following:

$$\delta\dot{\mathbf{u}} = -\mathbf{u} + \mathrm{P}_{\bar{\Omega}}(\mathbf{u} - G(\mathbf{u})) \tag{30}$$

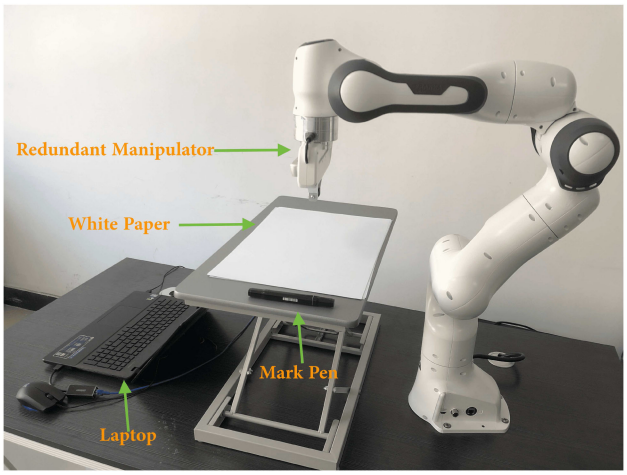

Fig. 4. Physical experiment platform.

where $\mathrm{P}_{\bar{\Omega}} = \{(\dot{\mathbf{q}}, \boldsymbol{\lambda}_1, \boldsymbol{\lambda}_2), \dot{\mathbf{q}} \in \Omega \subset \mathbb{R}^a, \boldsymbol{\lambda}_1 \in \mathbb{R}^{2b}, \boldsymbol{\lambda}_2 \in \mathbb{R}^c, c = 4\}$, and $G(\cdot)$ is defined as

$$G(\mathbf{u}) = G(\dot{\mathbf{q}}, \boldsymbol{\lambda}_1, \boldsymbol{\lambda}_2) = \begin{bmatrix} \dot{\mathbf{q}} + J^{\mathrm{T}} A^{\mathrm{T}} \boldsymbol{\lambda}_1 + H^{\mathrm{T}} \boldsymbol{\lambda}_2 \\ W - AJ\dot{\mathbf{q}} \\ -H\dot{\mathbf{q}} \end{bmatrix}. \tag{31}$$

Furthermore, we have the property

$$\nabla G = \frac{\partial G(\mathbf{u})}{\partial \mathbf{u}} = \begin{bmatrix} I & AJ & H \\ -J^{\mathrm{T}} A^{\mathrm{T}} & 0 & 0 \\ -H^{\mathrm{T}} & 0 & 0 \end{bmatrix} \tag{32}$$

and

$$\nabla G + \nabla G^{\mathrm{T}} = \begin{bmatrix} 2I & 0 & 0 \\ 0 & 0 & 0 \\ 0 & 0 & 0 \end{bmatrix} \tag{33}$$

where I represents an identity matrix. Since (33) is positive semidefinite, from the mean-value theorem it follows that there exists $G(l) - G(m) = \nabla G(n)(l - m)$ for any l, m, and n, when $n = \gamma l + (1 - \gamma)m \quad (0 < \gamma < 1)$. $G(\cdot)$ is a monotone function conducted from the following:

$$(l - m)^{\mathrm{T}}(G(l) - G(m)) = (l - m)^{\mathrm{T}} \nabla G(n)(l - m) \geq 0. \tag{34}$$

According to [14, Lemma 4], the state variable $\mathbf{u}$ in (30) is Lyapunov stable and globally converges to $\mathbf{u}^* = (\bar{\dot{\mathbf{q}}}^*, \boldsymbol{\lambda}_1^*, \boldsymbol{\lambda}_2^*)$ satisfying the following:

$$(\mathbf{u} - \mathbf{u}^*)^{\mathrm{T}} G(\mathbf{u}^*) \geq 0, \quad \forall \mathbf{u} \in \bar{\Omega}. \tag{35}$$

Furthermore, for any $\dot{\mathbf{q}} \in \Omega$, $\boldsymbol{\lambda}_1 \in \mathbb{R}^{2b}$, and $\boldsymbol{\lambda}_2 \in \mathbb{R}^4$ there exists

$$\begin{aligned}(\bar{\dot{\mathbf{q}}} - \bar{\dot{\mathbf{q}}}^*)^{\mathrm{T}}(-J^{\mathrm{T}} A^{\mathrm{T}} \boldsymbol{\lambda}_1 - H^{\mathrm{T}} \boldsymbol{\lambda}_2) + (\boldsymbol{\lambda}_1 - \boldsymbol{\lambda}_1^*)^{\mathrm{T}}(W - AJ\bar{\dot{\mathbf{q}}}) \\ + (\boldsymbol{\lambda}_2 - \boldsymbol{\lambda}_2^*)^{\mathrm{T}}(-H\bar{\dot{\mathbf{q}}}) \geq 0.\end{aligned} \tag{36}$$

Note that $\mathbf{u}$ in (30) converges to $\bar{\Omega}$, which means that $\mathbf{u}^*$ in (35) is in set $\bar{\Omega}$ as well. For convenience, let $S = \mathbf{u} - P_{\bar{\Omega}}(\mathbf{u})$ and design the Lyapunov function $V_1 = S^{\mathrm{T}} S/2$. Since $\dot{V}_1 = S\dot{\mathbf{u}} = -S^{\mathrm{T}}(\mathbf{u} - P_{\bar{\Omega}}(\mathbf{u} - G(\mathbf{u})))/\delta \leq 0$, and when $\mathbf{u} \in \bar{\Omega}$, there has $\dot{V}_1 = 0$, from which we can draw the conclusion that the state variables $\dot{\mathbf{q}}$, $\boldsymbol{\lambda}_1$, and $\boldsymbol{\lambda}_2$ of the RNN (22) can reach the stable states. Thus, the proof is complete.

V. Simulations, Physical Experiments, and Comparisons

In this section, simulations, physical experiments, and comparisons are presented to demonstrate the correctness, practicability, and innovation of the DDMFC scheme (20). First, simulations are carried out on MATLAB and the MindSpore framework, where the manipulator is given a path-tracking task with the end-effector force maintenance as the target, which means that the end-effector's orientation is expected to be unchanged. Then, physical experiments are conducted on a 7-DOF redundant manipulator named Franka Emika Panda. Finally, the DDMFC scheme (20) is compared with other controllers in the existing studies, which investigates the redundant manipulator from different perspectives.

A. Simulation Illustration

In the simulation, the scheme is carried out on the KUKA iiwa manipulator, which has 7 DOFs. The D-H parameters of the manipulator can be found in [15]. The manipulator is given a tricuspid valve path-tracking task with a constant contact force maintaining on the end-effector. The initial state of manipulator's joints is set to $[0, -0.2, 0, 2.5, 0, -0.5, 0]^{\mathrm{T}}$ rad. The contact force $\mathbf{f}_{\mathrm{d}}$ maintained by the end-effector is set to 0.1 N, and the stiffness coefficient of the object is 100. In order to compare the different performances in learning ability under different step-size of the RNN (22), the ϖ is set to 10^{-4}, 10^{-5}, and 10^{-6}, respectively. The initial value of $\boldsymbol{\lambda}_1$ and $\boldsymbol{\lambda}_2$ is generated by the random number from 0 to 0.1; the value of the parameter δ is set to 0.001; the joint velocity constraints of manipulator is $\dot{\mathbf{q}}^+ = -\dot{\mathbf{q}}^- = [0.5]_{7\times 1}$ rad/s.

Fig. 2 compares the learning ability when choosing different values of ϖ. Fig. 2(a) depicts the time history of the Jacobian matrix estimation error that ϖ is 10^{-4}. It can be seen from Fig. 2(a) that the estimation of the Jacobian matrix $\hat{J}$ has enormous fluctuations during the task and is not convergent to zero. Fig. 2(b) shows the enhancement of learning ability when ϖ is 10^{-5}, but the estimation error still fluctuates in the range of 0.1 and is not desirable. Fig. 2(c) shows the superior learning ability with a fast convergent rate when ϖ is 10^{-6}, of which the Jacobian matrix error converges to a tiny value within 10^{-3}. From Fig. 2, it can be conducted that the learning ability is improved with the decreasing of the step-size ϖ in the RNN (22), such that the real Jacobian matrix value is correctly estimated.

Subsequently, the control performance of the simulation experiments is displayed. The value of the step-size ϖ in the neural network (22d) is set to 10^{-6}, which can estimate the value of the Jacobian matrix accurately. The simulation results are shown in Fig. 3. As presented in Fig. 3(a), the manipulator's joint position fluctuates smoothly during the task. Fig. 3(b) displays the actual trajectory and desired trajectory of the end-effector. The trajectory generated by the manipulator during task execution is consistent with the desired trajectory well, and the joint's movement is smooth. Fig. 3(c) shows the time history

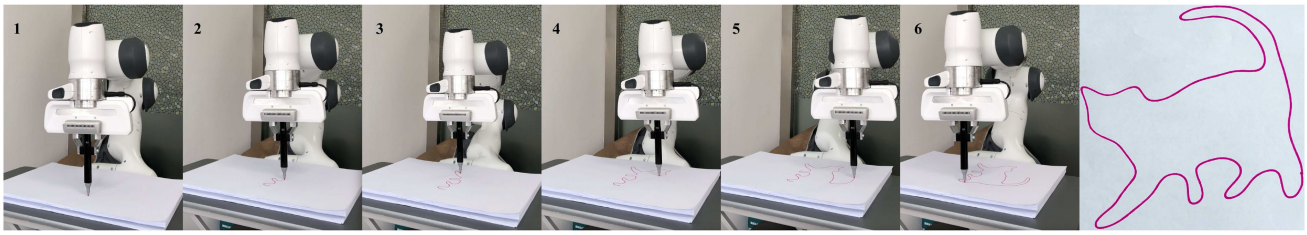

Fig. 5. Snapshots of the manipulator when performing the motion-force control task aided with the DDMFC scheme (20).

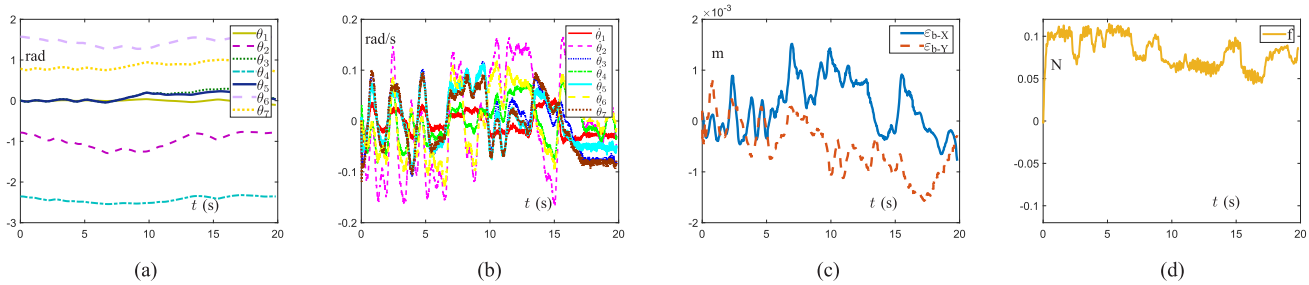

Fig. 6. Experiment results on Franka Emika Panda manipulator performing a trajectory tracking task with a cat-like trajectory. (a) Time history of joint angles. (b) Time history of joint velocities. (c) Time history of Position errors of the end-effector on *X* and *Y* axes. (d) Time history of contact force on the end-effector along the *Z*-axis.

of joint velocities within the range of physical constraints. Fig. 3(d) indicates the time history of joint angles during the task, and the manipulator is back to its initial position when finishing the task. Fig. 3(e) depicts the displacement error of the end-effector, which are fluctuating on the order of 10^{-4} m. Fig. 3(f) displays the deformation force of the end-effector along the *Z*-axis, which converges to the desired value dramatically; that is, the motion-force control task running on the manipulator is implemented accurately. In this sense, the effectiveness of the DDMFC scheme (20) is well validated.

B. Physical Experiments

To verify the effectiveness of the DDMFC scheme (20) in practical application, physical experiments are conducted on a 7-DOF redundant manipulator named Franka Emika Panda. The D-H parameters of the manipulator can be found in [20]. The initial state of the manipulator is $[0, -\pi/4, 0, -3\pi/4, 0, \pi/2, \pi/4, \pi/4]^{\mathrm{T}}$ rad, and the $\mathbf{f}_{\mathrm{d}} = 0.1$ N; the stiffness coefficient of the contact object is assumed as 100; the step-size of the learning law $\varpi = 10^{-6}$; the convergent rate δ of the RNN is set to 10^{-3}. The experiment's software environment is driven by the official C++ library libfranka built on the ubuntu 16.04 LTS operating system.

In the experiments, the Franka Emika Panda manipulator is given a motion-force control task, and a marker is clipped to the end-effector to draw the trajectory on the white paper. The manipulator is driven by joint velocity signals to track a cat-like trajectory within 20 s. Meanwhile, the manipulator's end-effector is maintaining a constant contact force $\mathbf{f}_{\mathrm{d}} = 0.1$ N. Fig. 4 depicts the experiment setup.

Fig. 5 depicts the time instants states of the manipulator during the task and the final trajectory of the task. We can conclude that the end-effector's orientation of the manipulator is unchanged during the task. Besides, the assigned trajectory tracking task is finished perfectly, and the end-effector returns to its start position precisely after finishing the task. Fig. 6 demonstrates the measured data of the manipulator during the physical experiment. Fig. 6(a) and (b) depicts the position and velocity in joint space of the manipulator during the experiments, respectively, which are continuous and smooth. Fig. 6(c) depicts the position error of the end-effector in base frame, fluctuating in the range of 2×10^{-3} m. Fig. 6(d) depicts the contact force on the end-effector along the *Z*-axis, and the contact force fluctuates in the range of 10^{-2} N slightly due to friction and measurement errors. In general, the physical experiment results successfully substantiate the feasibility and practicability of the DDMFC scheme (20).

C. Comparisons

In this subsection, the DDMFC scheme (20) is compared with other robot controllers in the existing studies [4], [8]–[10], [17]–[19]. Each controller has different research characteristics. The comparisons are conducted from the control characteristics and features. As shown in Table I, the DDMFC scheme (20) and controllers in [8], [9], [18], [19] achieve hybrid motion-force control. The proposed controller (20) is of great advantages in simultaneous learning and control for manipulators with unknown parameters compared with controllers in [9], [18], [19]. The controller in [8] also implements the learning and control but from a dynamic perspective. The controller (20) considers the end-effector maintaining and joint constraint avoidance in light

TABLE I
COMPARISONS AMONG DIFFERENT CONTROLLERS FOR MOTION-FORCE CONTROL AND LEARNING ABILITY OF REDUNDANT MANIPULATORS

	Motion Control	Force Control	Dynamics or Kinematics	Driven Signal	Effector Maintaining	Joint Constraint Avoidance	Structure Information ⋆
Controller (20)	Yes	Yes	Kinematics	Velocity	Yes	Yes	No
Controller in [4]	Yes	No	Kinematics	Velocity	No	No	Yes
Controller in [8]	Yes	Yes	Dynamics	Torque	No	No	No
Controller in [9]	Yes	Yes	Kinematics	Velocity	No	Yes	Yes
Controller in [10]	Yes	No	Kinematics	Velocity	Yes	No	No
Controller in [17]	Yes	No	Kinematics	Acceleration	No	Yes	Yes
Controller in [18]	Yes	Yes	Dynamics	Torque	No	No	Yes
Controller in [19]	Yes	Yes	Dynamics	Torque	No	No	Yes

⋆ "Structure information" means that whether full knowledge of the redundant manipulator is required or not.

of kinematics control. In this regard, the DDMFC scheme (20) can be considered as a meaningful innovation in the redundant manipulator control field.

VI. CONCLUSION

This article proposed a DDMFC scheme, which combined the learning and control parts of redundant manipulators. The scheme aimed to solve the motion-force control problem from a kinematic perspective when redundant manipulators' model parameters were unknown. The minimization of velocity norm had been regarded as the objective function, and the Jacobian matrix of redundant manipulators had been estimated precisely aided with data-driven technology. Besides, due to the manipulator's redundancy, the manipulator's physical constraints and end-effector orientation maintenance had been considered. The corresponding RNN for solving the learning problem and the control problem had been devised. Rigorous theoretical analysis had proved the learning and control abilities of the RNN. The simulation results and physical experiments had illustrated the efficiency and practicability of the DDMFC scheme. At last, comparisons with other controllers had revealed the advantages of the scheme. To the best of our knowledge, it is the first time that the motion-force control problem of redundant manipulators in the absence of model parameters is investigated. In the future, we will try to extend the data-driven approach to the orientation control of manipulator, which will also be applied to more practical scenarios.

REFERENCES

[1] X. Zhao, C. Ma, X. Xing, and X. Zheng, "A stochastic sampling consensus protocol of networked Euler-Lagrange systems with application to two-link manipulator," *IEEE Trans. Ind. Informat.*, vol. 11, no. 4, pp. 907–914, Aug. 2015.

[2] G. Du, Y. Liang, B. Gao, S. Al Otaibi, and D. Li, "A cognitive joint angle compensation system based on self-feedback fuzzy neural network with incremental learning," *IEEE Trans. Ind. Informat.*, vol. 17, no. 4, pp. 2928–2937, Apr. 2021.

[3] Q. Feng, Z. Li, J. Cai, and D. Guo, "Acceleration-level configuration adjustment scheme for robot manipulators," *IEEE Trans. Ind. Informat.*, vol. 17, no. 1, pp. 147–157, Jan. 2021.

[4] Z. Zhang and Z. Yan, "A varying parameter recurrent neural network for solving nonrepetitive motion problems of redundant robot manipulators," *IEEE Trans. Control Syst. Technol.*, vol. 27, no. 6, pp. 2680–2687, Nov. 2019.

[5] F. J. Comin, C. M. Saaj, S. M. Mustaza, and R. Saaj, "Safe testing of electrical diathermy cutting using a new generation soft manipulator," *IEEE Trans. Robot.*, vol. 34, no. 6, pp. 1659–1666, Dec. 2018.

[6] L. Roveda, G. Pallucca, N. Pedrocchi, F. Braghin, and L. M. Tosatti, "Iterative learning procedure with reinforcement for high-accuracy force tracking in robotized tasks," *IEEE Trans. Ind. Informat.*, vol. 14, no. 4, pp. 1753–1763, Apr. 2018.

[7] A. Owen-Hill, "The 7 best robot applications for a force sensor," *Robotiq*, Mar. 5, 2021. [Online]. Available: https://blog.robotiq.com/7-great-robot-applications-for-a-force-sensor

[8] Y. Li, C. Yang, W. Yan, R. Cui, and A. Annamalai, "Admittance-based adaptive cooperative control for multiple manipulators with output constraints," *IEEE Trans. Neural Netw. Learn. Syst.*, vol. 30, no. 12, pp. 3621–3632, Dec. 2019.

[9] Z. Xu, S. Li, X. Zhou, S. Zhou, T. Cheng, and Y. Guan, "Dynamic neural networks for motion-force control of redundant manipulators: An optimization perspective," *IEEE Trans. Ind. Electron.*, vol. 68, no. 2, pp. 1525–1536, Feb. 2021.

[10] S. Li, Z. Shao, and Y. Guan, "A dynamic neural network approach for efficient control of manipulators," *IEEE Trans. Syst., Man, Cybern., Syst.*, vol. 49, no. 5, pp. 932–941, May 2019.

[11] M. Liu, L. Chen, X. Du, L. Jin, and M. Shang, "Activated gradients for deep neural networks," *IEEE Trans. Neural Netw. Learn. Syst.*, to be published, doi: 10.1109/TNNLS.2021.3106044.

[12] Z. Zhang, S. Chen, X. Zhu, and Z. Yan, "Two hybrid end-effector posture-maintaining and obstacle-limits avoidance schemes for redundant robot manipulators," *IEEE Trans. Ind. Informat*. vol. 16, no. 2, pp. 754–763, Feb. 2020.

[13] Y. Zhang, J. Wang, and Y. Xia, "A dual neural network for redundancy resolution of kinematically redundant manipulators subject to joint limits and joint velocity limits," *IEEE Trans. Neural. Netw.*, vol. 14, no. 3, pp. 658–667, May 2003.

[14] X.-B. Gao, "Exponential stability of globally projected dynamic systems," *IEEE Trans. Neural Netw.*, vol. 14, no. 2, pp. 426–431, Mar. 2003.

[15] A. M. Kabir, K. N. Kaipa, J. Marvel, and S. K. Gupta, "Automated planning for robotic cleaning using multiple setups and oscillatory tool motions," *IEEE Trans. Autom. Sci. Eng.*, vol. 14, no. 3, pp. 1364–1377, Jul. 2017.

[16] H. K. Khalil, *Nonlinear Systems*, 3rd ed. Englewood Cliffs, NJ, USA: Prentice-Hall, 2001.

[17] L. Jin, Z. Xie, M. Liu, C. Ke, C. Li, and C. Yang, "Novel joint-drift-free scheme at acceleration level for robotic redundancy resolution with tracking error theoretically eliminated," *IEEE/ASME Trans. Mechatronics*, vol. 26, no. 1, pp. 90–101, Feb. 2021.

[18] C. Chen, Z. Liu, Y. Zhang, and S. Xie, "Coordinated motion/force control of multiarm robot with unknown sensor nonlinearity and manipulated object's uncertainty," *IEEE Trans. Syst., Man, Cybern., Syst.*, vol. 47, no. 7, pp. 1123–1134, Jul. 2017.

[19] W. Xu, T. Liu, and Y. Li, "Kinematics, dynamics, and control of a cable-driven hyper-redundant manipulator," *IEEE/ASME Trans. Mechatronics*, vol. 23, no. 4, pp. 1693–1704, Aug. 2018.

[20] D. Fu *et al.*, "Modified Newton integration algorithm with noise tolerance applied to robotics," *IEEE Trans. Syst., Man, Cybern., Syst*., to be published, doi: 10.1109/TSMC.2021.3049386.

Jialiang Fan received the B.E. degree in software engineering from Shandong University, Jinan, China, in 2019. He is currently working toward the M.E. degree in computer technology with the School of Information Science and Engineering, Lanzhou University, Lanzhou, China.

His main research interests include robotics, neural networks, intelligent information processing, artificial intelligence, and optimization theory.

Long Jin (Senior Member, IEEE) received the B.E. degree in automation and the Ph.D. degree in information and communication engineering from Sun Yat-sen University, Guangzhou, China, in 2011 and 2016, respectively.

He received a Postdoctoral training with the Department of Computing, The Hong Kong Polytechnic University, Hong Kong, from 2016 to 2017. In 2017, he joined the School of Information Science and Engineering, Lanzhou University, Lanzhou, China, as a Professor of Computer Science and Engineering. His current research interests include neural networks, robotics, optimization, and intelligent computing.

Prof. Jin is currently serving as an Editor for the *Neural Processing Letters*.

Zhengtai Xie received the B.E. degree in communication and information system in 2019 from Lanzhou University, Lanzhou, China, where he is currently working toward the Ph.D. degree in computer application technology.

His main research interests include robotics, neural networks, intelligent information processing, artificial intelligence, and optimization theory.

Shuai Li (Senior Member, IEEE) received the B.E. degree in precision mechanical engineering from the Hefei University of Technology, Hefei, China, in 2005, the M.E. degree in automatic control engineering from the University of Science and Technology of China, Hefei, in 2008, and the Ph.D. degree in electrical and computer engineering from the Stevens Institute of Technology, Hoboken, NJ, USA, in 2014.

His current research interests include dynamic neural networks, wireless sensor networks, robotic networks, machine learning, and other dynamic problems defined on a graph.

Dr. Li is on the Editorial Board of the *International Journal of Distributed Sensor Networks*.

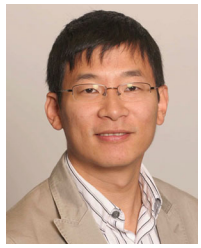

Yu Zheng (Senior Member, IEEE) received the B.E. degrees in mechanical engineering and computer science from Shanghai Jiao Tong University, Shanghai, China, in 2001, the M.S. and Ph.D. degrees in computer science from the University of North Carolina at Chapel Hill, Chapel Hill, NC, USA, in 2011 and 2014, respectively, and the Ph.D. degree in mechatronics from Shanghai Jiao Tong University, in 2007.

Between 2007 and 2009, he was a Postdoctoral Research Fellow with the Department of Mechanical Engineering, National University of Singapore, Singapore. He worked as a Lab Associate, a Research Associate, and finally a Postdoctoral Researcher with Disney Research Pittsburgh, Pittsburgh, PA, USA between 2010 and 2014. From 2014 to 2018, he was an Assistant Professor with the Department of Electrical and Computer Engineering, University of Michigan-Dearborn, Dearborn, MI, USA. He joined Tencent Robotics X, Shenzhen, China in September 2018 and currently is a Principal Research Scientist and the Team Lead with Control Center. His research interests include multicontact/multibody robotic systems, robotic grasping and manipulation, legged locomotion, and various algorithms for robotics.

Dr. Zheng serves as an Associate Editor for *IEEE Robotics and Automation Letters*.